OPTICA

X-ray magnetic circular dichroism spectroscopy at the Fe *L* edges with a picosecond laser-driven plasma source

Martin Borchert,[1] Dieter Engel,[1] Clemens von Korff Schmising,[1] Bastian Pfau,[1] Stefan Eisebitt,[1,2] and Daniel Schick[1,*]

[1]Max-Born-Institut für Nichtlineare Optik und Kurzzeitspektroskopie, Max-Born-Straße 2A, 12489 Berlin, Germany
[2]Technische Universität Berlin, Institut für Optik und Atomare Physik, Straße des 17. Juni 135, 10623 Berlin, Germany
*schick@mbi-berlin.de

Received 8 November 2022; revised 23 February 2023; accepted 6 March 2023; published 4 April 2023

Time-resolved x-ray magnetic circular dichroism (XMCD) enables a unique spectroscopic view on complex spin and charge dynamics in multi-elemental magnetic materials. So far, its application in the soft-x-ray range has been limited to synchrotron-radiation sources and free-electron lasers. By combining a laser-driven plasma source with a magnetic thin-film polarizer, we generate up to 30% circular polarization in the soft-x-ray regime, enabling the first XMCD spectroscopy at the Fe *L* edges in a laser laboratory, to our knowledge. Our approach can be readily adapted to other transition metal *L* and rare earth *M* absorption edges, and with a temporal resolution of < 10 ps, a wide range of ultrafast magnetization studies can be realized.

https://doi.org/10.1364/OPTICA.480221

1. INTRODUCTION

X-ray magnetic circular dichroism (XMCD) [1–3] is an established and powerful tool to probe magnetic properties in a variety of material systems relevant to solid-state physics, chemistry, biology, and material science [4]. It relies on the strong dichroic absorption of circularly polarized light when tuned close to the vicinity of spin-split core-to-valence-band transitions, spanning from the extreme ultraviolet (XUV) up to the hard-x-ray regime. Especially in the soft-x-ray range, the XMCD effect exhibits a large magnetic contrast across the transition metal (TM) $L_{2,3}(2p \rightarrow 3d)$ and rare earth (RE) $M_{4,5}(3d \rightarrow 4f)$ absorption edges [5]. In addition to its element and site specificity, soft-XMCD spectroscopy allows to separate the orbital and spin contributions of the local magnetic moments via so-called sum rules [6–8]. The absorption-based XMCD contrast has enabled further experimental x-ray techniques, e.g., magnetization-sensitive microscopy [9] and holography [10].

Today, circularly polarized soft x-rays are readily available at synchrotron-radiation facilities worldwide, providing full polarization control, high photon flux, and wavelength tunability with superb spectral resolution for tackling various experimental tasks. For the ultrafast magnetism community, the availability of short-pulse sources (femto- to few picosecond pulse duration) with inherent circular polarization in the soft-x-ray range is, however, rather limited to one laser-slicing source [11] and one free-electron laser [12] (FEL), with upgrades of several soft-x-ray FEL beamlines being planned or already under construction. Laser-driven higher-harmonic generation (HHG) sources have gained popularity and importance for time-resolved XMCD studies [13–15], generating circular polarization by two-color driving fields [16,17] or phase shifters [18,19]. However, due to the extremely low flux of these sources [20] at photon energies corresponding to the TM *L* edges and above, a true laboratory-based alternative for time-resolved XMCD experiments in the soft-x-ray range is still lacking.

In this paper, we describe the first table-top XMCD experiment across the Fe *L* edges around 700 eV with < 10 ps temporal resolution, based on a laboratory source. Specifically, the broadband (50–1500 eV) emission of a laser-driven plasma x-ray source (PXS) is exploited [21]. For that, we create a sufficiently large net degree of circular polarization of the—initially *randomly polarized*—soft x-rays by dichroic absorption through a ferrimagnetic thin-film polarizer [22,23] with intrinsic out-of-plane (OOP) magnetization. The broadband characteristic of this approach enables the measurement of XMCD spectra across the entire spin–orbit pair of Fe *L* edges in a single acquisition with a signal-to-noise ratio (SNR) comparable to typical bending-magnet beamlines at synchrotron-radiation facilities. In addition, the short-pulse characteristics and the possibility for extension to other photon energies, such as RE *M* edges, render this approach a versatile alternative for static and time-resolved XMCD experiments to study a large set of phenomena in ultrafast magnetism, such as all-optical magnetic switching (AOS) [24] or photo-induced phase transitions [25].

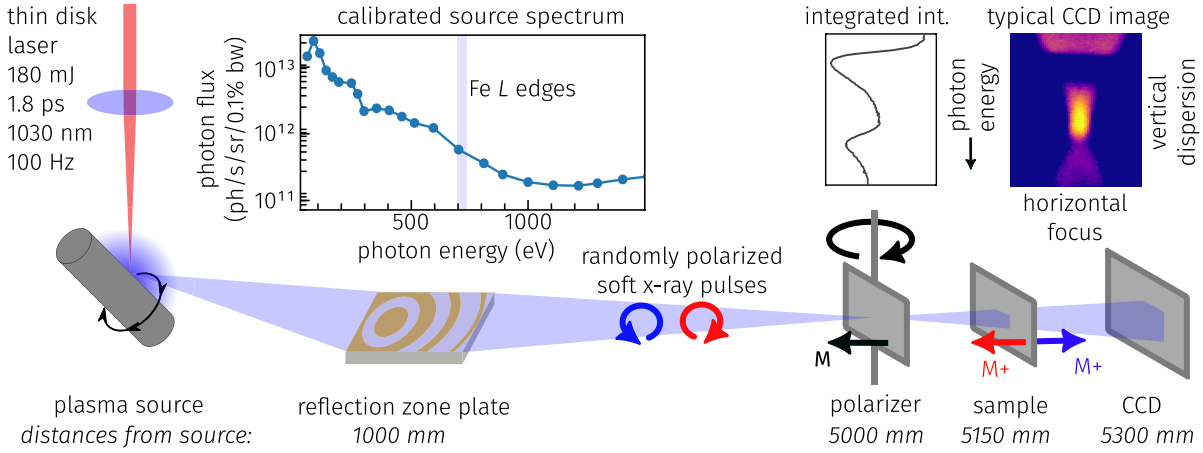

Fig. 1. Schematic overview of the experimental setup. Short and intense laser pulses are focused onto a spinning tungsten cylinder, generating a plasma that emits short, broadband soft-x-ray pulses (< 10 ps, 50–1500 eV); see inset. A slice of the spectrum is captured by a reflection zone plate and horizontally focused, while vertically dispersed through a magnetic thin film polarizer and a subsequent sample, both under normal incidence, onto a CCD camera. The orientation of the polarizer and its magnetization can be changed by a rotational stage, while the magnetization of the sample is altered by an external electromagnet.

2. CONCEPT

The driver for the soft-x-ray source is an in-house-developed double-stage thin-disk-amplified laser, producing pulses with a duration of 1.8 ps full width at half maximum (FWHM) at a wavelength of 1030 nm with a pulse energy of 180 mJ at 100 Hz repetition rate [26]. At the laser focus of $\approx 15\,\mu$m diameter FWHM, a spinning tungsten cylinder is placed under an angle of 45°. Upon laser excitation of the tungsten target, a plasma is generated that emits the aforementioned broadband x-ray radiation into the full solid angle [27]. We use a reflective zone plate (RZP) [28] as the *single* optical element, designed to collect, disperse, and focus the full spectrum across the Fe L_3 and L_2 edges from the point-like laser-plasma source with a diameter of $\approx 40\,\mu$m FWHM through the polarizer and subsequent sample as depicted in Fig. 1. For the RZP's design energy of $E = 715$ eV, a horizontal focus of 200 µm and an energy resolution of $\Delta E/E > 550$ along the vertical dimension are obtained at a photon flux of 10^7 ph/s/eV. For photon energies off the design value, decreasing spatial and spectral focusing results in the hourglass-like beam profile of 3.5 mm (horizontal) × 4 mm (vertical) of the soft x-rays at the polarizer and sample position as shown in the right inset in Fig. 1. Resonances of other elements can be readily accessed by additional RZPs mounted on the same manipulator.

We describe the emission from the PXS in the basis of left (σ^-) and right (σ^+) circularly polarized photons [29]. Due to the *thermal* processes involved in the generation, the amounts of σ^- and σ^+ polarized photons are equal [30]. This ratio is also maintained after reflection off the RZP, which exhibits a negligible difference (< 1%) in reflectivity for vertical and horizontal field components. When transmitting the σ^- and σ^+ x-rays through a ferro- or ferrimagnetic polarizer of thickness d_p, they will exhibit different transmissions $T^{\pm}(M_p, E)$ due to the XMCD effect:

$$T_p^{\pm}(M_p, E) = \exp\left[-2kd_p\left(\beta(E) \pm M_p\Delta\beta(E)\right)\right], \quad (1)$$

where $\beta(E)$ and $\Delta\beta(E)$ are the photon-energy-dependent electronic and magnetic absorptive parts of the polarizer's refractive index, respectively, and M_p is the magnitude of the polarizer magnetization, projected onto the wave vector of the x-rays with magnitude k. Thus, the transmitted light becomes partially circularly polarized as quantified by the polarization factor

$$P(M_p, E) = \frac{T^-(M_p, E) - T^+(M_p, E)}{T^-(M_p, E) + T^+(M_p, E)} = \tanh\left[2kd_pM_p\Delta\beta_p(E)\right], \quad (2)$$

which is equivalent to the well-known XMCD asymmetry [2]. As evident from Eq. (2), a net circular polarization is observable only at photon energies, where $\Delta\beta(E) \neq 0$ and for a finite magnetization M_p. While the magnitude of $\Delta\beta(E)$ is material specific, the largest $M_p = \pm 1$ is obtained for saturated ferro- and ferrimagnetic films with OOP magnetization at normal incidence. The degree of polarization can be enhanced by increasing the thickness of the polarizer, but at the same time, the total transmission, c.f. Eq. (1), will drop exponentially. To define an optimum between the degree of polarization and the transmitted light intensity in dependence on the material thickness, the figure of merit TP^2 [22] is applied.

We choose the ferrimagnetic $Gd_{0.24}Fe_{0.76}$ alloy for the polarizer and sample, as it exhibits an OOP magnetization in remanence, as verified by optical Kerr measurements. The thicknesses of the polarizer and sample are $d_p = 100$ nm and $d_s = 55$ nm, respectively, both being below the optimum of TP^2 at the Fe L_3 absorption edge; see Supplement 1. Both films are seeded and capped with 3 nm of Ta and grown onto a 50 nm thick SiN membrane. Their clear aperture of 4 mm × 4 mm allows to transmit the full vertically dispersed soft-x-ray spectrum across the Fe L_3 and L_2 edges in a single shot. Rotating the polarizer by 180° normal to the beam axis inverts its magnetization M_p with respect to the beam propagation direction, allowing to easily invert the helicity of the transmitted x-rays. The magnetization of the sample M_s can be altered by an external magnetic field, and the transmission of the polarizer and sample, dispersed along the vertical coordinate, is captured with a subsequent CCD camera.

From the two transmissions $T_{\text{tot}}^+(E) = T_{\text{tot}}(M_p, +M_s, E)$ and $T_{\text{tot}}^-(E) = T_{\text{tot}}(M_p, -M_s, E)$, of the initially randomly polarized soft x-rays through the polarizer (fixed M_p) and sample (two sample magnetization states $\pm M_s$), we derive (c.f. Supplement 1) the

total asymmetry as

$$A_{\mathrm{tot}}(M_p, M_s, E) = \frac{T^-_{\mathrm{tot}}(E) - T^+_{\mathrm{tot}}(E)}{T^-_{\mathrm{tot}}(E) + T^+_{\mathrm{tot}}(E)} \tag{3}$$

$$= \tanh\left[2kd_p M_p \Delta\beta_p(E)\right] \tanh\left[2kd_s M_s \Delta\beta_s(E)\right] \tag{4}$$

$$\underset{\sim}{\propto} P(M_p, E)\, M_s \Delta\beta_s(E). \tag{5}$$

In a first approximation, A_{tot} scales linearly with the degree of circular polarization P, induced by the ferrimagnetic polarizer and sample magnetization component M_s parallel to the x-ray wave vector.

3. RESULTS AND DISCUSSION

To confirm the existence and quantify the degree of circular polarization of the PXS emission after passing through the ferrimagnetic polarizer of fixed magnetization M_p, we probe the total, dispersed transmission spectra $T^{\pm}_{\mathrm{tot}}$ behind the sample across the Fe L_3 and L_2 edges for the two saturation states $M_s = \pm 1$ at external magnetic fields of $B = \pm 100$ mT. The average of both dichroic spectra is plotted in Fig. 2 on a logarithmic scale. The two insets zoom in to the two individual spectra $T^{\pm}_{\mathrm{tot}}$ at the L_3 and L_2 edges. They show a significant difference in absorption between the two magnetic saturation states of the sample—a clear indication of the XMCD effect and hence of the circular polarization of the impinging x-rays. Both spectra have been recorded within a total integration time of only 170 s each, thus less than 6 min total with an SNR $>$ 200 across the whole spectral range. Details on data acquisition and correction procedures are presented in the Methods section of Supplement 1.

We quantify the degree of polarization $P(M_p, E)$ at the Fe L_3 and L_2 edges by fitting the experimental spectra with magnetic scattering simulations [31,32]. They are based on the sample and polarizer geometries, their experimentally determined $\beta(E)$ and $\Delta\beta(E)$ [33,34], as well as the individual magnetization magnitudes $M_{p,s}$ of the polarizer and sample, respectively. The simulations have been first bench-marked by XMCD spectra of the sample taken at a synchrotron-radiation beamline; see Supplement 1 for more details. The best-fit result, taking the spectral resolution $E/\Delta E$ of the spectrometer into account, yields a maximum degree of circular polarization of 30% at the Fe L_3 edge and -7 % at the Fe L_2 edge, with a magnetization of the polarizer of only $M_p = 0.48 < 1$. We attribute this reduction to magnetically dead layers in the ferrimagnetic $Gd_{24}Fe_{76}$ film and/or to magnetic domains having formed, while it was kept in remanence without an external field after being initially saturated once. Applying such an external magnetic field by an electromagnet would constantly saturate the polarizer magnetization at $M_p = \pm 1$, and even allow for fast polarization control.

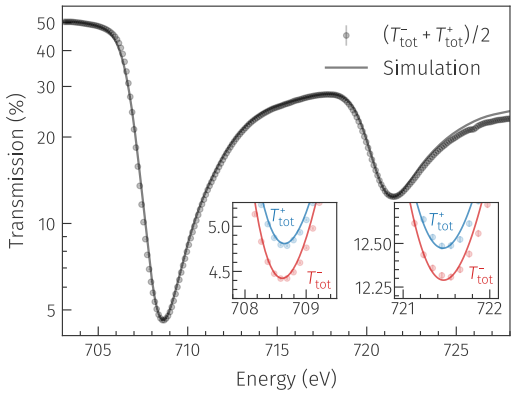

Fig. 2. Average of the two total transmissions T^-_{tot} and T^+_{tot}, resembling a typical x-ray-absorption spectrum (XAS). The two insets zoom into the Fe L_3 (left) and L_2 (right) absorption edges and show the individual transmitted intensities T^-_{tot} and T^+_{tot} for the two saturated magnetization states of the sample. A significant XMCD contrast is visible. The solid lines represent magnetic scattering simulations and the dots the experimental data.

Further analyzing the above data, we determine the total asymmetry A_{tot}, c.f. Eq. (3), and compare it to the simulations, as shown in Fig. 3. The experimentally observed peak asymmetries at the Fe L_3 and L_2 edges of about 4% and 1%, respectively, are in good agreement with the theoretical predictions and constitute the first laboratory-based XMCD spectroscopy in the soft-x-ray range. The experimental asymmetries are, however, constricted by the non-optimal degree of polarization of the soft x-rays as well as by the limited spectral resolution of the setup. Without both of these limitations, the scattering simulations predict even up to 4.5-times larger total asymmetries of 17.5% and 2.5% at the Fe L_3 and L_2 edges, respectively, for the chosen geometries.

Interestingly, the total asymmetry A_{tot} has the same sign at both L edges, although $\Delta\beta(L_3) < 0$ and $\Delta\beta(L_2) > 0$. This is best explained by reinspecting Eq. (4), in which the sign of $\Delta\beta(E)$ determines both the helicity of the x-rays when passing the polarizer as well as the sign of the probed XMCD of the sample at a given photon energy E. Due to the multiplication of both factors in Eq. (4) the sign of the total asymmetry A_{tot} is independent of the sign of $\Delta\beta$. However, it is possible to change the sign of A_{tot} by changing only the sign of the polarization factor $P(M_p, E)$ at a given photon energy E. This is accomplished by inverting its magnetization M_p, i.e., by rotating the polarizer by 180°. The resulting inverted asymmetry is also plotted in Fig. 3 and is nearly perfectly symmetric to the initial curve.

Finally, to provide an application scenario for our technique, we probe the dispersed, total transmission T_{tot} for a fixed polarizer magnetization M_p, while scanning the sample magnetization via the applied magnetic field from $M_s = -1$ to $M_s = +1$. By plotting the peak intensity, integrated over a 4 eV bandwidth across each absorption L edge, against the applied magnetic field, we obtain

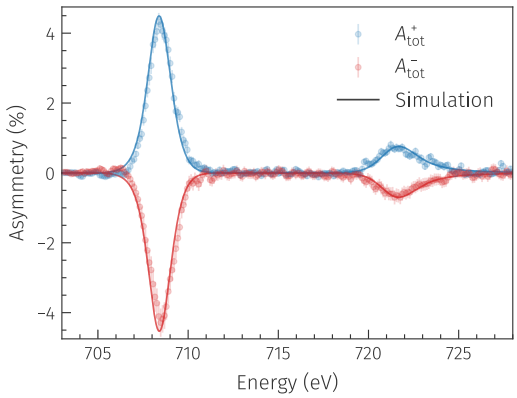

Fig. 3. Total asymmetries $A^+_{\mathrm{tot}} = A_{\mathrm{tot}}(M_p = +1)$ and $A^-_{\mathrm{tot}} = A_{\mathrm{tot}}(M_p = -1)$ behind the polarizer and sample, calculated from the experimental dichroic spectra from Fig. 2 via Eq. (3). The solid lines represent magnetic scattering simulations and the dots the experimental data. The colors represent two different polarizer magnetization directions $\pm M_p$.

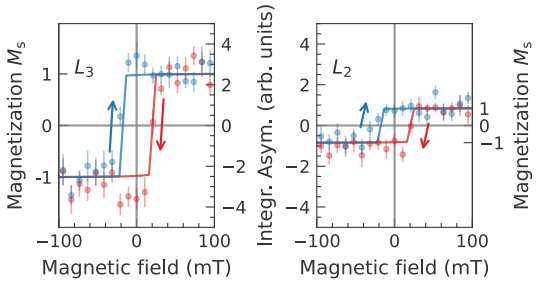

Fig. 4. Transmission $T_{tot}(M_s)$ behind the polarizer and sample at the Fe L_3 (left) and L_2 (right) absorption edges, while scanning the sample's magnetization M_s in a hysteresis loop. The inner y axis corresponds to the integrated total asymmetries across the absorption edges. The two different colors correspond to the two scan directions of the hysteresis loop, as indicated by the arrows; the solid lines represent magneto-optical Kerr-effect (MOKE) measurements, scaled to the measurement data (dots) as a guide to the eye.

the expected square-shaped magnetic hysteresis loops, as depicted in Fig. 4. Magneto-optical Kerr effect (MOKE) measurements from the same sample are overlaid as a guide to the eye. We find the expected behavior of the hysteresis scans with a smaller amplitude at the Fe L_2 compared to the L_3 edge, but with the same symmetry, i.e., observation of positive asymmetry for positive field and vice versa. The latter observation can again be explained by the different signs of the polarization factor at both edges. Note that the integration time per data point in the hysteresis scans was reduced by an order of magnitude to only 17 s, compared to the spectra shown in Figs. 2 and 3, and that they are both obtained simultaneously.

The first realization of a picosecond, laser-driven XMCD spectrometer reaching the TM L edges is an important step towards opening this powerful technique for a broader community. Next, we want to discuss the applicability of our approach in terms of available photon flux and SNR, as well as of spectral and temporal resolution, in particular for the field of ultrafast magnetism research.

The SNR > 200 of the dichroic spectra across the Fe L_3 and L_2 edges was achieved within only a few minutes of total integration time. This data quality is comparable to current bending-magnet beamlines at synchrotron-radiation facilities, c.f. Supplement 1, and is the result of the spectroscopic *white-light* scheme and the possible self-normalization to non-resonant regions, when evaluating these broadband spectra. It is hence possible to acquire low-noise asymmetry spectra with partially circularly polarized soft x-rays, which can be fitted against magnetic scattering simulations with very high sensitivity. These simulations in combination with a calibrated polarizer even allow for determining the *absolute* XMCD of the investigated sample.

Despite the remarkable SNR of the results presented, the setup can be improved for XMCD spectroscopy in several aspects. As already mentioned above, magnetic field control at the polarizer would ensure its full performance and allow for fast polarization switching. Even more important, we have identified intensity fluctuations of the PXS as the main source of noise in the experiment, since the detectable photon flux, even at the strongly absorbing Fe L_3 edge, is still well above the noise level of the CCD camera. These fluctuations mainly originate from mechanical instabilities of the target cylinder and can be tackled by improved suspension and new target concepts, such as metallic tapes or wires, as well as by applying additional normalization schemes, e.g., by a spectrally resolved I_0 monitor [19]. While reducing noise, it is also possible to increase the signal, namely, the XMCD asymmetry, by increasing the polarizer thickness d_p and hence the degree of circular polarization P. From our simulations, we predict an increase of the maximum degree of circular polarization at the Fe L_3 edge for a 200 nm (400 nm) thick polarizer of 85% (99%) at a total transmission of 1.0% (0.04%) for the current 50 nm sample, as seen in the Polarizer Analysis section in Supplement 1. Although the detectable photon flux is drastically reduced by one to two orders of magnitude for such polarizer thicknesses, it will at the same time allow for single photon counting schemes, using novel area detector generations [35,36], for which the noise of the experiment is finally approaching the shot noise limit. Moreover, the 100 Hz repetition rate of the experiment is currently determined by the laser system, while the mechanical source and detection would easily allow for repetition rates of > 1000 Hz. Hence, using commercially available laser systems [37], increasing the available photon flux by more than one order of magnitude is feasible.

While the available photon flux and SNR are certainly well suited for static experiments, we want to consider the particular value of an XMCD spectrometer with < 10 ps temporal resolution in ultrafast magnetism research, as alternative sources are rare. While many fundamental processes during laser-driven spin dynamics occur on a sub-picosecond time scale [38–40], many collective phenomena such as magnetic phase transitions [25], spin precessions [41], and AOS [42,43] share intrinsic time scales of a few pico- up to nanoseconds. For instance, the realization of magnetic switching exploiting few-picosecond laser or current pump pulses [44–46] is of high technological relevance for better CMOS integrability. To that end, our setup provides a new laboratory-based tool to specifically follow the sub-lattice magnetization of typical heterostructures and alloys, made of TM and RE metals, during such picosecond magnetization switching dynamics and can provide relevant insights into the underlying mechanisms, which are otherwise hardly accessible, e.g., via optical methods. As in such experiments the magnetic information is usually determined by integrating the XMCD asymmetry over the full magnetically sensitive absorption edges (e.g., Fe L_3 and L_2 edges), the moderate spectral resolution of $E/\Delta E \approx 550$ and the photon-energy-dependent degree of circular polarization do not hamper the application of our method. Extending our approach to a broader class of materials, e.g., for oxides, must allow for variations of the dichroic absorption spectra in the soft-x-ray range, due to changes of the coordination and valency of the relevant magnetic ions compared to elemental metals. For solid-state samples, the required spectral overlap of the dichroic absorption for the polarizer and sample can, however, always be fulfilled by using the same material for both of them.

4. CONCLUSION

So far, all studies on magnetization dynamics in the lower picosecond regime, exploiting the XMCD effect at photon energies above the water window (> 500 eV), require the use of large-scale facilities. As an alternative, we have realized the first XMCD spectroscopy setup in the soft-x-ray regime at the Fe L edges at a laser-driven source. Our concept can be readily extended to other photon energies, namely, to the magnetically relevant TM L and RE M edges from approx. 500–1500 eV. The high SNR of the presented XMCD spectra in combination with the few-picosecond

temporal resolution will enable the study of a wide range of magnetization dynamics relevant for, e.g., AOS or magneto-structural phase transitions. The high flexibility in the sample environment, the short iteration cycles, e.g., for sample customization, and the high availability of a laboratory-based ultrafast XMCD setup will allow for detailed and systematic studies of time- and element-resolved spin dynamics.

Funding. Leibniz-Gemeinschaft (Leibniz Junior Research Group J134/2022); Deutsche Forschungsgemeinschaft (TRR227 project A02).

Acknowledgment. M.B., C.v.K.S., and S.E. thank the DFG for funding through TRR227 project A02. D.S. thanks the Leibniz Association for funding through the Leibniz Junior Research Group J134/2022.

Author Contributions. D.S. conceived the experiment together with M.B., B.P., and S.E.; D.E. grew the samples; M.B. carried out the experiments and evaluated the data; M.B. and D.S. discussed the results and wrote the paper with contributions from all other co-authors.

Disclosures. The authors declare no competing interests.

Data availability. The data sets generated during and/or analyzed during the current study are available from the corresponding author upon reasonable request.

Supplemental document. See Supplement 1 for supporting content.

REFERENCES

1. G. van der Laan, B. T. Thole, G. A. Sawatzky, J. B. Goedkoop, J. C. Fuggle, J.-M. Esteva, R. Karnatak, J. P. Remeika, and H. A. Dabkowska, "Experimental proof of magnetic x-ray dichroism," Phys. Rev. B **34**, 6529–6531 (1986).
2. G. Schütz, W. Wagner, W. Wilhelm, P. Kienle, R. Zeller, R. Frahm, and G. Materlik, "Absorption of circularly polarized x rays in iron," Phys. Rev. Lett. **58**, 737–740 (1987).
3. J. Stöhr, "Exploring the microscopic origin of magnetic anisotropies with X-ray magnetic circular dichroism (XMCD) spectroscopy," J. Magn. Magn. Mater. **200**, 470–497 (1999).
4. G. van der Laan and A. I. Figueroa, "X-ray magnetic circular dichroism—a versatile tool to study magnetism," Coord. Chem. Rev. **277-278**, 95–129 (2014).
5. J. B. Kortright, D. D. Awschalom, J. Stöhr, S. D. Bader, Y. U. Idzerda, S. S. Parkin, I. K. Schuller, and H. C. Siegmann, "Research frontiers in magnetic materials at soft X-ray synchrotron radiation facilities," J. Magn. Magn. Mater. **207**, 7–44 (1999).
6. B. T. Thole, P. Carra, F. Sette, and G. van der Laan, "X-ray circular dichroism as a probe of orbital magnetization," Phys. Rev. Lett. **68**, 1943–1946 (1992).
7. P. Carra, B. T. Thole, M. Altarelli, and X. Wang, "X-ray circular dichroism and local magnetic fields," Phys. Rev. Lett. **70**, 694–697 (1993).
8. J. Stöhr and H. König, "Determination of spin- and orbital-moment anisotropies in transition metals by angle-dependent x-ray magnetic circular dichroism," Phys. Rev. Lett. **75**, 3748–3751 (1995).
9. J. Stöhr, Y. Wu, B. D. Hermsmeier, M. G. Samant, G. R. Harp, S. Koranda, D. Dunham, and B. P. Tonner, "Element-specific magnetic microscopy with circularly polarized x-rays," Science **259**, 658–661 (1993).
10. S. Eisebitt, J. Lüning, W. F. Schlotter, M. Lörgen, O. Hellwig, W. Eberhardt, and J. Stöhr, "Lensless imaging of magnetic nanostructures by X-ray spectro-holography," Nature **432**, 885–888 (2004).
11. K. Holldack, J. Bahrdt, A. Balzer, *et al.*, "FemtoSpeX: a versatile optical pump–soft X-ray probe facility with 100 fs X-ray pulses of variable polarization," J. Synchrotron Radiat. **21**, 1090–1104 (2014).
12. D. J. Higley, A. H. Reid, Z. Chen, L. L. Guyader, O. Hellwig, A. A. Lutman, T. Liu, P. Shafer, T. Chase, G. L. Dakovski, A. Mitra, E. Yuan, J. Schlappa, H. A. Dürr, W. F. Schlotter, and J. Stöhr, "Femtosecond x-ray induced changes of the electronic and magnetic response of solids from electron redistribution," Nat. Commun. **10**, 5289 (2019).
13. F. Siegrist, J. A. Gessner, M. Ossiander, C. Denker, Y.-P. Chang, M. C. Schröder, A. Guggenmos, Y. Cui, J. Walowski, U. Martens, J. K. Dewhurst, U. Kleineberg, M. Münzenberg, S. Sharma, and M. Schultze, "Light-wave dynamic control of magnetism," Nature **571**, 240–244 (2019).
14. F. Willems, C. von Korff Schmising, C. Strüber, D. Schick, D. W. Engel, J. K. Dewhurst, P. Elliott, S. Sharma, and S. Eisebitt, "Optical inter-site spin transfer probed by energy and spin-resolved transient absorption spectroscopy," Nat. Commun. **11**, 871 (2020).
15. M. Hofherr, S. Häuser, J. K. Dewhurst, P. Tengdin, S. Sakshath, H. T. Nembach, S. T. Weber, J. M. Shaw, T. J. Silva, H. C. Kapteyn, M. Cinchetti, B. Rethfeld, M. M. Murnane, D. Steil, B. Stadtmüller, S. Sharma, M. Aeschlimann, and S. Mathias, "Ultrafast optically induced spin transfer in ferromagnetic alloys," Sci. Adv. **6**, eaay8717 (2020).
16. O. Kfir, P. Grychtol, E. Turgut, R. Knut, D. Zusin, D. Popmintchev, T. Popmintchev, H. Nembach, J. M. Shaw, A. Fleischer, H. Kapteyn, M. Murnane, and O. Cohen, "Generation of bright phase-matched circularly-polarized extreme ultraviolet high harmonics," Nat. Photonics **9**, 99–105 (2015).
17. T. Fan, P. Grychtol, R. Knut, *et al.*, "Bright circularly polarized soft X-ray high harmonics for X-ray magnetic circular dichroism," Proc. Natl. Acad. Sci. USA **112**, 14206–14211 (2015).
18. B. Vodungbo, A. B. Sardinha, J. Gautier, G. Lambert, C. Valentin, M. Lozano, G. Iaquaniello, F. Delmotte, S. Sebban, J. Lüning, and P. Zeitoun, "Polarization control of high order harmonics in the EUV photon energy range," Opt. Express **19**, 4346 (2011).
19. K. Yao, F. Willems, C. von Korff Schmising, C. Strüber, P. Hessing, B. Pfau, D. Schick, D. Engel, K. Gerlinger, M. Schneider, and S. Eisebitt, "A tabletop setup for ultrafast helicity-dependent and element-specific absorption spectroscopy and scattering in the extreme ultraviolet spectral range," Rev. Sci. Instrum. **91**, 093001 (2020).
20. T. Feng, T. Feng, T. Feng, A. Heilmann, A. Heilmann, M. Bock, L. Ehrentraut, T. Witting, H. Yu, H. Stiel, S. Eisebitt, and M. Schnürer, "27 w 2.1 μm OPCPA system for coherent soft x-ray generation operating at 10 khz," Opt. Express **28**, 8724–8733 (2020).
21. D. Schick, M. Borchert, J. Braenzel, H. Stiel, J. Tümmler, D. E. Bürgler, A. Firsov, C. V. K. Schmising, B. Pfau, and S. Eisebitt, "Laser-driven resonant magnetic soft-x-ray scattering for probing ultrafast antiferromagnetic and structural dynamics," Optica **8**, 1237–1242 (2021).
22. J. B. Kortright, S.-K. Kim, T. Warwick, and N. V. Smith, "Soft x-ray circular polarizer using magnetic circular dichroism at the Fe L3 line," Appl. Phys. Lett. **71**, 1446–1448 (1997).
23. B. Pfau, C. M. Günther, R. Könnecke, E. Guehrs, O. Hellwig, W. F. Schlotter, and S. Eisebitt, "Magnetic imaging at linearly polarized x-ray sources," Opt. Express **18**, 13608–13615 (2010).
24. C. D. Stanciu, F. Hansteen, A. V. Kimel, A. Kirilyuk, A. Tsukamoto, A. Itoh, and T. Rasing, "All-optical magnetic recording with circularly polarized light," Phys. Rev. Lett. **99**, 047601 (2007).
25. G. Li, R. Medapalli, J. H. Mentink, R. V. Mikhaylovskiy, T. G. H. Blank, S. K. K. Patel, A. K. Zvezdin, T. Rasing, E. E. Fullerton, and A. V. Kimel, "Ultrafast kinetics of the antiferromagnetic-ferromagnetic phase transition in Ferh," Nat. Commun. **13**, 2998 (2022).
26. R. Jung, J. Tümmler, and I. Will, "Regenerative thin-disk amplifier for 300 mJ pulse energy," Opt. Express **24**, 883–887 (2016).
27. I. Mantouvalou, K. Witte, D. Grötzsch, M. Neitzel, S. Günther, J. Baumann, R. Jung, H. Stiel, B. Kanngießer, and W. Sandner, "High average power, highly brilliant laser-produced plasma source for soft x-ray spectroscopy," Rev. Sci. Instrum. **86**, 035116 (2015).
28. M. Brzhezinskaya, A. Firsov, K. Holldack, T. Kachel, R. Mitzner, N. Pontius, J.-S. Schmidt, M. Sperling, C. Stamm, A. Föhlisch, and A. Erko, "A novel monochromator for experiments with ultrashort x-ray pulses," J. Synchrotron Radiat. **20**, 522–530 (2013).
29. P. A. M. Dirac, *The Principles of Quantum Mechanics*, 4th ed. (Oxford University, 1930).
30. H. Legall, H. Stiel, U. Vogt, H. Schoennagel, P.-V. Nickles, J. Tuemmler, F. Scholz, and F. Scholze, "Spatial and spectral characterization of a laser produced plasma source for extreme ultraviolet metrology," Rev. Sci. Instrum. **75**, 4981 (2004).
31. D. Schick, "UDKM1Dsim–a Python toolbox for simulating 1D ultrafast dynamics in condensed matter," Comput. Phys. Commun. **266**, 108031 (2021).
32. M. Elzo, E. Jal, O. Bunau, S. Grenier, Y. Joly, A. Ramos, H. Tolentino, J. Tonnerre, and N. Jaouen, "X-ray resonant magnetic reflectivity of stratified magnetic structures: eigenwave formalism and application to a W/Fe/W trilayer," J. Magn. Magn. Mater. **324**, 105–112 (2012).

33. C. T. Chen, Y. U. Idzerda, H.-J. Lin, N. V. Smith, G. Meigs, E. Chaban, G. H. Ho, E. Pellegrin, and F. Sette, "Experimental confirmation of the x-ray magnetic circular dichroism sum rules for iron and cobalt," Phys. Rev. Lett. **75**, 152–155 (1995).
34. J. F. Peters, J. Miguel, M. A. de Vries, O. M. Toulemonde, J. B. Goedkoop, S. S. Dhesi, and N. B. Brookes, "Soft x-ray resonant magneto-optical constants at the Gd $M_{4,5}$ and Fe $L_{2,3}$ edges," Phys. Rev. B **70**, 224417 (2004).
35. A. Bergamaschi, M. Andrä, R. Barten, *et al.*, "The Mönch detector for soft x-ray, high-resolution, and energy resolved applications," Synchrotron Radiat. News **31**, 11–15 (2018).
36. C. Dullin, J. Albers, G. Tromba, M. Andrä, M. Ramilli, and A. Bergamaschi, "Mönch detector enables fast and low-dose free-propagation phase-contrast computed tomography of in situ mouse lungs," J. Synchrotron Radiat. **25**, 565–569 (2018).
37. Y. Pfaff, M. Rampp, C. Herkommer, R. Jung, C. Y. Teisset, S. Klingebiel, and T. Metzger, "Thin-disk based regenerative chirped pulse amplifier with 550 mJ pulse energy at 1 kHz repetition rate," in *Laser Congress (ASSL, LAC)* (Optica Publishing Group, 2021), paper AM2A.5.
38. M. Battiato, K. Carva, and P. M. Oppeneer, "Superdiffusive spin transport as a mechanism of ultrafast demagnetization," Phys. Rev. Lett. **105**, 027203 (2010).
39. J. K. Dewhurst, P. Elliott, S. Shallcross, E. K. U. Gross, and S. Sharma, "Laser-induced intersite spin transfer," Nano Lett. **18**, 1842–1848 (2018).
40. M. Beens, R. A. Duine, and B. Koopmans, "s–d model for local and non-local spin dynamics in laser-excited magnetic heterostructures," Phys. Rev. B **102**, 054442 (2020).
41. D. M. Burn, S. L. Zhang, G. Q. Yu, Y. Guang, H. J. Chen, X. P. Qiu, G. van der Laan, and T. Hesjedal, "Depth-resolved magnetization dynamics revealed by x-ray reflectometry ferromagnetic resonance," Phys. Rev. Lett. **125**, 137201 (2020).
42. I. Radu, K. Vahaplar, C. Stamm, T. Kachel, N. Pontius, H. A. Dürr, T. A. Ostler, J. Barker, R. F. L. Evans, R. W. Chantrell, A. Tsukamoto, A. Itoh, A. Kirilyuk, T. Rasing, and A. V. Kimel, "Transient ferromagnetic-like state mediating ultrafast reversal of antiferromagnetically coupled spins," Nature **472**, 205–208 (2011).
43. F. Steinbach, N. Stetzuhn, D. Engel, U. Atxitia, C. von Korff Schmising, and S. Eisebitt, "Accelerating double pulse all-optical write/erase cycles in metallic ferrimagnets," Appl. Phys. Lett. **120**, 112406 (2022).
44. J. Igarashi, Q. Remy, S. Iihama, G. Malinowski, M. Hehn, J. Gorchon, J. Hohlfeld, S. Fukami, H. Ohno, and S. Mangin, "Engineering single-shot all-optical switching of ferromagnetic materials," Nano Lett. **20**, 8654–8660 (2020).
45. Y. Yang, R. B. Wilson, J. Gorchon, C. H. Lambert, S. Salahuddin, and J. Bokor, "Ultrafast magnetization reversal by picosecond electrical pulses," Sci. Adv. **3**, 1–7 (2017).
46. E. Grimaldi, V. Krizakova, G. Sala, F. Yasin, S. Couet, G. Sankar Kar, K. Garello, and P. Gambardella, "Single-shot dynamics of spin–orbit torque and spin transfer torque switching in three-terminal magnetic tunnel junctions," Nat. Nanotechnol. **15**, 111–117 (2020).